Numerical modelling of centrifuge dynamic tests on embedded cantilevered retaining walls

Riccardo Conti*

Summary

This paper presents the results from the numerical simulation of two dynamic centrifuge tests carried out on embedded cantilevered walls in dry sand, reconstituted at two different values of relative density. Plane strain analyses were performed using an advanced constitutive model for the soil, in which the set of model parameters was calibrated on the basis of standard laboratory tests. The results show that advanced numerical modelling provides a good description of the seismic response of embedded retaining walls: very good agreement between numerical predictions and centrifuge data is obtained in terms of accelerations, while some discrepancies are observed in terms of displacements and bending moments in the walls, mainly due to experimental factors not taken into account in the numerical analyses. The dynamic behaviour of embedded cantilevered retaining walls is strongly related to the redistribution of the stress state around the excavation induced by the inertia forces into the soil. More specifically, permanent rotations of the wall induce a progressive mobilization of the soil passive resistance and a consistent increase of the internal forces into the wall. Furthermore, significant displacements can be attained during an earthquake even for maximum accelerations smaller than the limit equilibrium critical value.

Keywords: retaining walls, earthquake, numerical modelling, centrifuge tests, earth pressures, displacements, seismic design

Introduction

Extensive damage to earth retaining structures and adjacent buildings has been observed in a number of past earthquakes, most of them attributed to liquefaction of saturated backfill [PIANC, 2001; Day, 2002; Fang *et al.*, 2003]. As a result, in the last years many works have been devoted to the experimental [Dewoolkar *et al.*, 2001; Marketos and Madabhushi, 2004; Conti *et al*, 2012; Aversa *et al.*, 2015] and numerical [Madabhushi and Zeng, 2007; Callisto *et al.*, 2008; Dewoolkar *et al.*, 2009; Atik and Sitar, 2010; Cilingir *et al.*, 2011; Conti *et al.*, 2014] modelling of retaining walls under seismic loadings, in order to understand better the dynamic behaviour of such structures and to develop more rational procedures for the design practice.

Experimental works carried out on reduced-scale models allow to investigate the seismic response of geotechnical systems under ideal conditions, in which the initial state of the soil (usually a homogeneous layer) and the hydraulic conditions are imposed, and both the dynamic input motion and the boundary conditions are well defined. However, despite the fact that dynamic tests on reduced-scale models allow to identify many important phenomena and provide critical validation tools for numerical and analytical studies, they do not always shed light into the physical mechanisms affecting the observed behaviour. Two of the main reasons are: (i) not all the relevant quantities for the problem at hand can be measured at the same time during one test; (ii) dynamic model tests are usually too expensive to enable extensive parametric studies, in which the influence of different factors on the response of the system can be investigated.

A deeper insight into these physical mechanisms can be obtained from advanced numerical analyses (FEM or FDM), which usually provide a more comprehensive view of all the variables relevant for the problem, and can be extended to more general or complex conditions, taking into account different input motions and varying layouts or stratigraphy. Nevertheless, most factors for the numerical modelling of geotechnical systems under dynamic conditions seem to be still under debate, such as the definition of the input motion [Kwok *et al.*, 2007] and of suitable free-field boundary conditions [Kontoe *et al.*, 2009], and the selection of an appropriate time integration scheme [Kontoe *et al.*, 2008]. Along these lines, the choice of an adequate constitutive model for the soil is among the most critical issues.

A number of constitutive models have been developed to reproduce the behaviour of non-cohesive soils under cyclic loading. A detailed review is reported in Andrianopoulos *et al.* [2010a] and Zhang and Wang [2012]. Some of the most important requirements a constitutive model should satisfy can be summarised as follows: the ability to reproduce ad-

* Associate Professor, University of Rome Niccolò Cusano, Italy

 DOI:10.19199/2017.2.0557-1405.031

equately (i) the nonlinear and hysteretic behaviour of the soil with increasing deformation, (ii) the static and dynamic liquefaction related to excess pore pressure build-up in undrained loading and (iii) the evolution of soil fabric during cyclic shearing; (iv) the attainment of critical state conditions at large deviatoric strains; (v) the use of a single set of model parameters for any initial relative density or confining pressure; (vi) the possibility to calibrate model parameters from the results of standard laboratory tests.

Some of the constitutive models proposed in the literature provide a good qualitative description of the response of sands under small to large cyclic shear deformations, but most of them lack quantitative accuracy; furthermore, their predictive capabilities are usually verified only at single element level, and not in the simulation of more complex boundary value problems.

As far as retaining walls are concerned, experimental data from centrifuge tests have been used recently to ascertain the accuracy of numerical predictions obtained using advanced constitutive soil models [LING *et al.*, 2004; MADABHUSHI and ZENG, 2007; DEWOOLKAR *et al.*, 2008; ATIK and SITAR, 2010].

This paper focuses on the numerical simulation of two centrifuge tests on a pair of embedded cantilevered retaining walls in dry sand, reconstituted at two different values of the relative density [CONTI *et al.*, 2012]. Based on the experimental evidence, CONTI *et al.* [2012] have shown that the dynamic response of embedded cantilevered walls does not depend only on the current earthquake intensity, but also on the entire loading history applied to the structure. In other words, the wall will experience neither significant permanent displacements nor increments of the residual internal forces during an earthquake if a stronger event has occurred before. Moreover, significant displacements were measured even for maximum accelerations smaller than the critical limit equilibrium value, corresponding to full mobilisation of the soil strength. This last evidence has a crucial implication in the performance-based design of embedded cantilevered walls, according to which the permanent displacement of the structure under an earthquake of given maximum acceleration must be computed. As a matter of fact, while the NEWMARK [1965] rigid-block analysis can be used to compute seismic permanent displacements of gravity retaining walls [RICHARDS and ELMS, 1979; WHITMAN, 1990; CONTI *et al.*, 2013], well-established and reliable simplified procedures are still missing for the case of embedded cantilevered retaining walls.

The constitutive model proposed by ANDRIANOPOULOS *et al.* [2010a; 2010b], and implemented in the finite difference code FLAC [ITASCA, 2005], is adopted for the soil. The main objective of this work is twofold: (i) to validate the constitutive model, the performance of which in boundary value problems was discussed only by ANDRIANOPOULOS *et al.* [2010a] with reference to the VELACS project [1993]; (ii) to interpret the physical phenomena observed experimentally on the basis of the more comprehensive results provided by the numerical analyses.

After a brief description of the two centrifuge model tests, the main constitutive ingredients of the soil model are presented. The calibration procedure for the model parameters, starting from the results of a series of standard laboratory tests, is described in detail together with the subsequent validation procedure, carried out both at the element level and using 1-D wave propagation analyses. Finally, results from plane strain numerical simulations are discussed in order to clarify some of the physical mechanisms affecting the seismic behaviour of embedded cantilevered retaining walls.

Centrifuge model tests

A number of centrifuge dynamic tests were carried out on reduced scale models of pairs of retaining walls in dry sand, either cantilevered or propped against each other by one level of support near the top, using the beam centrifuge of the University of Cambridge [CONTI *et al.*, 2012]. In this paper, two experiments are discussed, namely test CW1 and CW2 on embedded cantilevered walls, carried out at a centrifugal acceleration of 80 *g*. The models were prepared within an equivalent shear beam container [ZENG and SCHOFIELD, 1996]. The main geometrical quantities and the relative densities of the sand are reported in Table I, where h is the excavation depth, d is the embedment depth, S is the excavation width and Z is the thickness of the soil layer.

Retaining walls were modelled using aluminium alloy plates (density, $\rho = 2700$ kg/m^3; Young modulus, $E = 68.5$ GPa; Poisson's ratio, $\nu = 0.3$) with a thickness of 3.18 mm. A standard fine silica sand was used, namely Leighton Buzzard, Fraction E Sand 100/170. The specific gravity of the sand is $G_S = 2.65$, its maximum and minimum voids ratio are 1.014 and 0.613, respectively, and its critical friction angle is $\phi_{cv} = 32°$ [TAN, 1990].

Tab. I – Geometry of centrifuge model tests, at model scale (Figures in brackets [ ] are prototype scale: m).
Tab. I – Geometria dei modelli realizzati in centrifuga, alla scala del modello (valori tra parentesi [ ] sono alla scala del prototipo: m).

Test	D_r	h	d	Z	S
	[%]	[mm]	[mm]	[mm]	[mm]
CW1	84	50 [4]	50 [4]	200 [16]	75 [6]
CW2	53	50 [4]	50 [4]	200 [16]	75 [6]

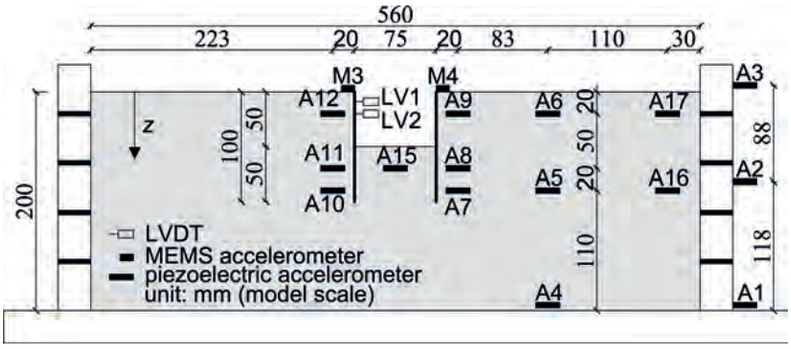

Fig. 1 – Test CW1: transducers layout.
Fig. 1 – Test CW1: disposizione della strumentazione.

Instrumentation was used to measure accelerations of the walls and at different locations in the model and on its boundaries, bending moments and horizontal displacements of the walls. As an example, figure 1 shows the layout of instrumentation for test CW1.

During each test, the model was subjected to a series of five trains of approximately sinusoidal waves with different nominal frequencies, f_{inp}, and amplitudes, a_{max}, and a constant duration of 32 s at prototype scale (see Tab. II). The input accelerations were applied at the base of the models in the horizontal direction. As an example, figure 2 shows the acceleration time history and the Fourier amplitude spectrum of earthquake EQ3 applied during test CW1.

In the following, accelerations are positive rightwards, while horizontal displacements and rotations of the walls are positive towards the excavation. All results are presented at prototype scale, unless explicitly stated. For sake of clarity, the main scale factors in geotechnical centrifuge modelling [MUIR WOOD, 2004] are reported in table III, where N is the ratio between the centrifugal and the gravity acceleration.

Constitutive model for the soil

The constitutive model adopted for the soil was developed by ANDRIANOPOULOS *et al.* [2010a; 2010b] within the framework of bounding surface plasticity and critical state soil mechanics, to simulate the mechanical behaviour of non-cohesive soils under small to large cyclic deformations. The main ingredients of the model, mostly derived from the original works by MANZARI AND DAFALIAS [1997] and PAPADIMITRIOU *et al.* [2001], are: (i) the existence of three conical surfaces in the stress space (critical state, bounding and dilatancy), interrelated through the state parameter ψ [BEEN and JEFFERIES, 1985]; (ii) kinematic hardening; (iii) a non-linear hysteretic formulation for the "elastic" moduli, which defines the shear modulus degradation and the hysteretic damping increase at small-medium shear strains; (iv) a scalar multiplier

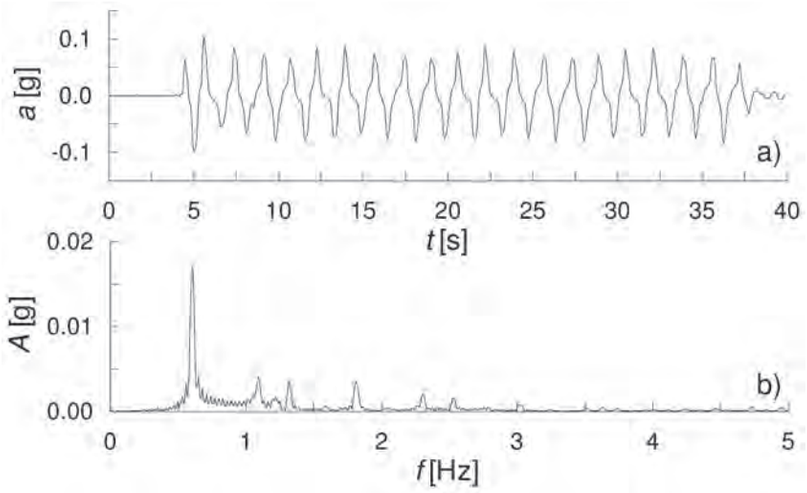

Fig. 2 – Test CW1, EQ3: a) acceleration time history; b) Fourier spectrum of the input signal.
Fig. 2 – Test CW1, EQ3: a) storia temporale delle accelerazioni; b) spettro di Fourier delle ampiezze relativi al segnale di ingresso.

Tab. II – Earthquake features (prototype scale).
Tab. II – Caratteristiche dei terremoti applicati in centrifuga (scala del prototipo).

TEST	EQ1		EQ2		EQ3		EQ4		EQ5	
	f_{inp} [Hz]	a_{max} [g]	f_{inp} [Hz]	a_{max} [g]	f_{inp} [Hz]	a_{max} [g]	f_{inp} [Hz]	a_{max} [g]	f_{inp} [Hz]	a_{max} [g]
CW1	0.50	0.08	0.75	0.17	0.63	0.10	0.75	0.18	0.63	0.17
CW2	0.38	0.05	0.50	0.07	0.63	0.13	0.75	0.15	0.63	0.14

Tab. III – Main scale factors in geotechnical centrifuge modelling.
Tab. III – Principali fattori di scala per la modellazione in centrifuga di problemi geotecnici.

quantity	scale factor
length	$1/N$
time (dynamic)	$1/N$
acceleration	N
stress	1
strain	1
force/unit length	$1/N$

for the plastic modulus, taking into account globally the sand fabric evolution during shearing. Note that, as the yield surface is not defined in the model, and hence no elastic domain exists, the term "elastic" used throughout the paper, and derived from ANDRIANOPOULOS *et al.* [2010a], refers simply to the behaviour of the soil at small strains.

The evolution equations defining the constitutive model are discussed in detail in many works (see *e.g.* MANZARI and DAFALIAS, 1997; PAPADIMITRIOU *et al.*, 2001; PAPADIMITRIOU and BOUCKOVALAS, 2002; ANDRIANOPOULOS *et al.*, 2010a], and therefore they are not reported in this paper. Some details on the calibration procedure adopted for the model parameters and on the subsequent validation of the model performance are presented in the following.

Calibration of model parameters

The constitutive model requires the definition of 13 parameters, which can be calibrated from the interpretation of standard laboratory tests (see *e.g.* PAPADIMITRIOU *et al.*, 2001; ANDRIANOPOULOS *et al.*, 2010a; CONTI *et al.*, 2014]. In this work, the model parameters were calibrated using the experimental data presented by VISONE [2008], referring to a number of laboratory tests carried out on samples of Leighton Buzzard Sand 100/170, reconstituted at different values of relative density. The complete set of laboratory tests is reported in table IV, where D_{r0} is the initial relative density and p'_0 is the initial effective mean pressure, while table V presents the corresponding set of values for the model parameters. For sake of clarity, the constitutive equations used for the calibration of some parameters are recalled in figure 3.

The parameters M_c and M_e define the slope of the Critical State Line (CSL) in the triaxial plane $q : p'$ of the stress invariants, while Γ and λ define the CSL in the $e : \ln p'$ plane. These parameters were obtained from undrained triaxial extension tests (TX-EU), drained triaxial compression tests (TX-CD) and drained triaxial compression tests at constant

Tab. IV – Laboratory testing programme [VISONE, 2008].
Tab. IV – Programma delle prove di laboratorio [VISONE, 2008].

Test		p'_0 [kPa]	D_{r0} [%]
TX-CU	Undrained TX Compression	200 ÷ 400	29 ÷ 31
TX-EU	Undrained TX Extension	200 ÷ 400	28 ÷ 30
TX-CD	Drained TX Compression	100 ÷ 200	81 ÷ 70
TX-CDp	Drained TX Compression at const. p'	100 ÷ 200 ÷ 400	76 ÷ 77 ÷ 81
RC	Resonant Column	30-400	58
RC	Resonant Column	30-100	47
RC	Resonant Column	40-200	52
RC	Resonant Column	50-400	71
TS	Torsional Shear	100 ÷ 200 ÷ 400	48 ÷ 54 ÷ 75

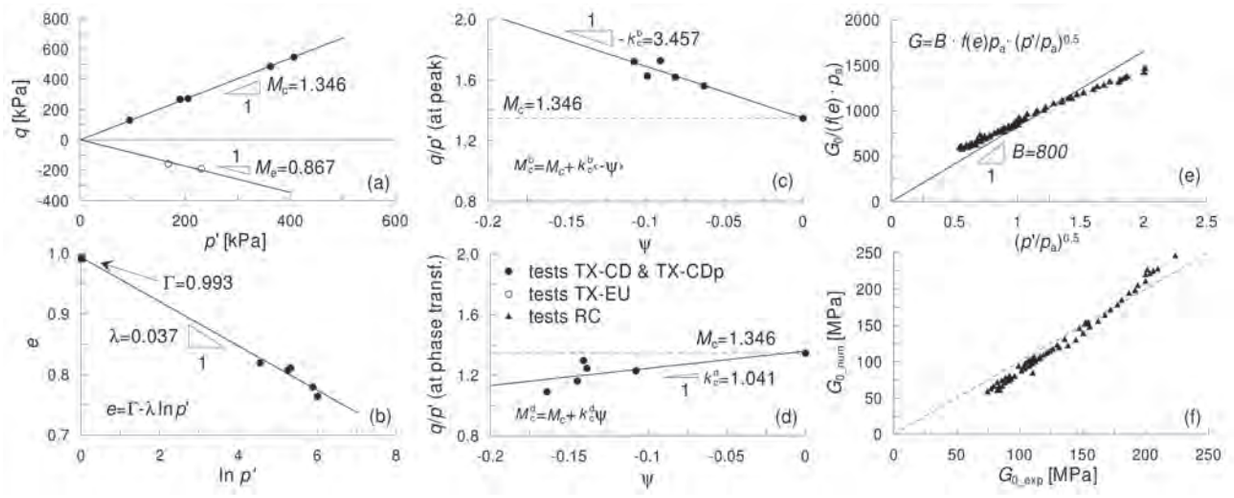

Fig. 3 – Calibration of model parameters from experimental data.
Fig. 3 – Taratura dei parametri del modello a partire dai dati sperimentali.

mean effective stress (TX-CDp), where a critical state was attained (see Fig. 3a, b).

The parameters k_c^b and k_c^d, which relate the bounding and the dilatancy surface to the critical state surface in the triaxial plane through the state parameter ψ [Been and Jefferies, 1985], were obtained from TX-CD and TX-CDp tests, by correlating the deviatoric stress ratio q/p' at the peak and at the phase transformation, respectively, to the values of ψ at which they are attained (see Fig. 3c, d).

Constant B, which defines the shear modulus at small strains, was estimated from RC tests carried out at different values of effective mean pressure and void ratio (see Fig. 3e, f). As observed by Papadimitriou *et al.* [2001], values of B obtained from small strain measurements are usually too large for an accurate simulation of monotonic loading. Accordingly, a reduced value of B (= 600) was used for the numerical simulation of both the TX-CD tests (single element analyses) and the static stage (swing-up) of the centrifuge tests (2-D analyses).

The parameters a_1 and γ_1 define the shear modulus degradation curve: γ_1 is related to the volumetric threshold shear strain, which ranges from 0.0065% to 0.025% for non-plastic soils [Vucetic, 1994], and a_1 is the corresponding value of G/G_0. In this work we set γ_1 = 0.025% and a_1 = 0.50 (Fig. 4), which are derived from the best fit of available centrifuge data [Conti and Viggiani, 2012] and provide a close match with literature data for non-plastic

Tab. V – Model parameters.
Tab. V – Parametri del modello costitutivo.

Parameter	Physical meaning	Value
Γ	Void ratio at critical state (p'=1kPa)	0.825
λ	Slope of CSL in the e-ln$p$' plane	0.037
M_c	Deviatoric stress ratio at critical state in triaxial compression (TXC)	1.346
M_e	Deviatoric stress ratio at critical state in triaxial extension (TXE)	0.867
k_c^b	Effect of ψ on peak deviatoric stress ratio (TXC)	3.457
k_c^d	Effect of ψ on dilatancy deviatoric stress ratio (TXC)	1.041
ν	Poisson's ratio	0.3
B	Elastic shear modulus constant	800
a_1	Non-linearity of elastic shear modulus	0.5 [0.85]
g_1	Reference shear strain for non-linearity of elastic shear modulus	0.00025
A_0	Dilatancy constant	1
h_0	Plastic modulus constant	50000
N_0	Fabric evolution constant	30000

Tab. VI – Maximum leftward accelerations during the earthquakes [g].
Tab. VI – Accelerazioni massime (verso sinistra) registrate durante i terremoti [g].

test	#	EQ1		EQ2		EQ3		EQ4		EQ5	
		exp	num	exp	num	exp	num	exp	num	exp	num
CW1	A1	0.08	0.08	0.13	0.13	0.10	0.10	0.17	0.17	0.16	0.16
	A6	0.11	0.10	0.20	0.21	0.13	0.14	0.26	0.26	0.23	0.24
	A12	0.11	0.10	0.20	0.24	0.13	0.15	0.26	0.27	0.25	0.26
CW2	A1	0.05	0.05	0.07	0.07	0.12	0.12	0.14	0.14	0.14	0.14
	A6	0.07	0.06	0.10	0.09	0.17	0.18	0.22	0.21	0.23	0.21
	A12	0.07	0.06	0.09	0.09	0.15	0.16	0.20	0.21	0.20	0.22

soils [VUCETIC and DOBRY, 1991]. As will be shown in the following section, the value $a_1 = 0.85$, which corresponds to the best fit of RC and TS data [VISONE, 2008], was not used in the 2-D analyses. Indeed, the behaviour of the soil during the dynamic centrifuge tests shows a more rapid degradation of the shear modulus than that reported by VISONE [2008].

The dilatancy constant, A_0, and the plastic modulus constant, h_0, were computed with a trial-and-error procedure, by fitting numerically the stress-strain response observed during TX-CD tests. Finally, in absence of direct measurements, a value of 0.3 was used for the Poisson's ratio, ν, while the value of the fabric constant, N_0, was chosen within the typical range provided by ANDRIANOPOULOS *et al.* [2010a].

Validation of the model

The ability of the constitutive model to reproduce the mechanical behaviour of the soil along monotonic loading paths was tested through the simulation, at the element level, of two drained triaxial compression tests (TX-CD), carried out at two different values of the initial consolidation pressure, namely LBS07 (p'_0 = 100 kPa) and LBS08 (p'_0 = 200 kPa). Figure 5 shows a quite good agreement between model predictions and experimental data.

The performance of the constitutive model during dynamic loading was verified through 1-D wave propagation analyses, in which the horizontal acceleration time histories recorded at the base of the model container during test CW1 (accelerometer A1) were applied at the bottom of a 1-D soil column. The horizontal accelerations computed from 1-D analyses were compared with those recorded in the centrifuge model by transducers A5 and A6, which are sufficient away from the walls to be considered representative of free-field soil conditions.

Figure 6 shows a comparison between numerical and experimental accelerations (accelerometer A6) during earthquakes EQ1 and EQ4. Numerical analyses were carried out adopting two different degradation curves for the shear modulus, that is $a_1 = 0.50$ and $a_1 = 0.85$. The choice of a_1 clearly does not affect the numerical predictions for EQ1 (Fig. 6a,b), in which the maximum applied acceleration is 0.08g, while the high frequency components of motion are amplified unrealistically during the stronger earthquake EQ4 when a_1 is set equal to 0.85 (Fig. 6 c,d). This observation, which is even more evident at higher accelerations (see *e.g.* CONTI, 2010), results from the fact that the shear modulus degradation curve derived from the best fit of RC and TS data does not describe adequately the non-linear behaviour exhibited by the soil with increasing strain.

The good agreement between measured accelerations and those computed from 1-D wave propagation analyses, which was obtained also for test CW2, shows that the dynamic interaction between the container and the soil layer does not play a significant role in the amplification phenomena observed during these centrifuge tests. It follows that 2-D plane strain analyses can be performed using standard periodic boundaries [ZIENKIEWICZ *et al.*, 1988] instead of modelling explicitly the container boundary conditions [ILANKATHARAN and KUTTER, 2008], thus simplifying considerably the numerical simulations.

Numerical model

Two-dimensional plane-strain finite difference analyses were carried out at the model scale, by simulating both the (static) swing-up stage, during which the centrifugal acceleration into the model is increased from 1 *g* to 80 *g*, and the subsequent dynamic stages. Figure 7 shows the mesh adopted for the two tests, with a total of 448 elements and a minimum size of 10 mm near the walls. The refinement of the grid was chosen in order to not influence the numerical results during both the static and the dynamic stages. Moreover, the element size Δl always guarantees an accurate wave transmission through the model, that is $\Delta l \leq \lambda/8$ [KUHLEMEYER and LYSMER, 1973], where $\lambda = V_S/f_{max}$ is the wavelength associated with the highest frequency of the input signals (f_{max} = 480 Hz at model scale), and V_S is the shear wave ve-

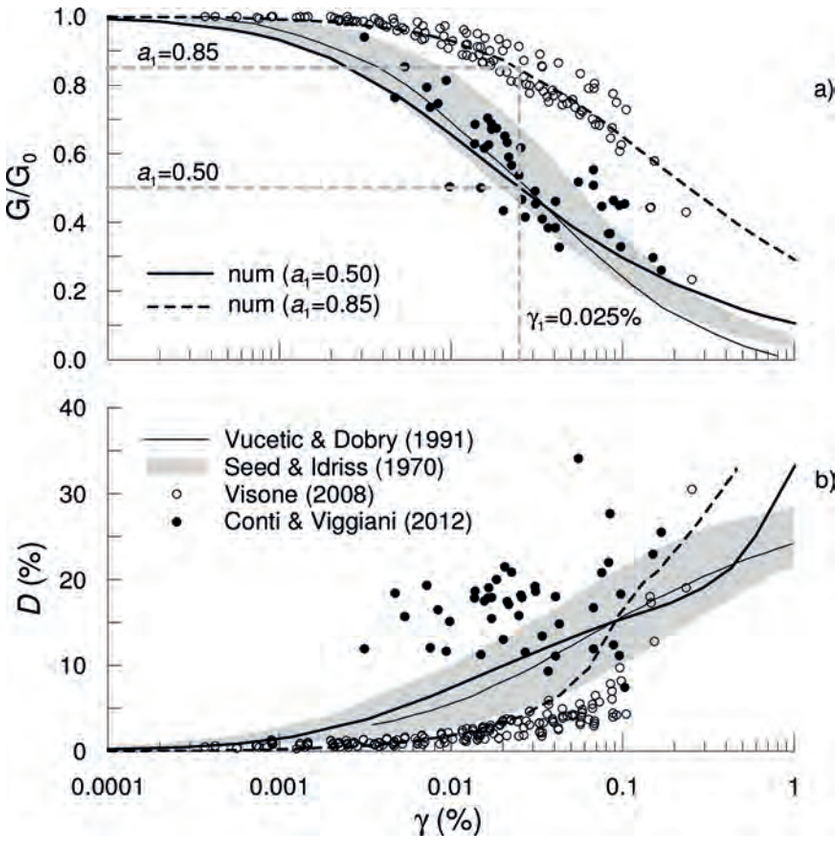

Fig. 4 – Shear modulus degradation and damping curves: calibration of model parameters from laboratory [VISONE, 2008] and centrifuge [CONTI and VIGGIANI, 2012] data.

Fig. 4 – Curva di decadimento del modulo di rigidezza a taglio e dello smorzamento: taratura dei parametri del modello a partire dai risultati delle prove di laboratorio [VISONE, 2008] e delle prove in centrifuga [CONTI e VIGGIANI, 2012].

locity corresponding to a shear strain of about 0.2% ($G/G_0 = 0.2$).

The structural elements were modelled as elastic isotropic beams. The walls were connected to the grid nodes with elastic-perfectly plastic interfaces, with a friction angle $\delta = 12°$ [MADABHUSHI and ZENG, 2007] and a normal and shear stiffness $k_s = k_n = 2\times10^7$ kN/m^2/m, which is about ten times the equivalent stiffness of the stiffest neighbouring zone [ITASCA, 2005].

The initial stress state was prescribed in terms of the earth pressure coefficient at rest $\sigma'_h/\sigma'_v = K_0$ (= 1-sinϕ_{cv}), while an initial void ratio $e_0 = 0.68$ (D_r = 84%) and $e_0 = 0.80$ (D_r = 53%) was adopted for test CW1 and CW2 respectively. Moreover, an increased value $e_0 = 0.84$ (D_r = 42%) was used in test CW1 for the soil elements immediately behind the walls and below dredge level (gray elements in Fig. 7) to take into account the fact that automatic sand pouring, during model preparation, usually results in lower values of the actual relative density of the soil close to the walls. This value of relative density, also measured in other centrifuge tests (see *e.g.* CONTI *et al.*, 2012), was chosen to have a better match with the experimental data.

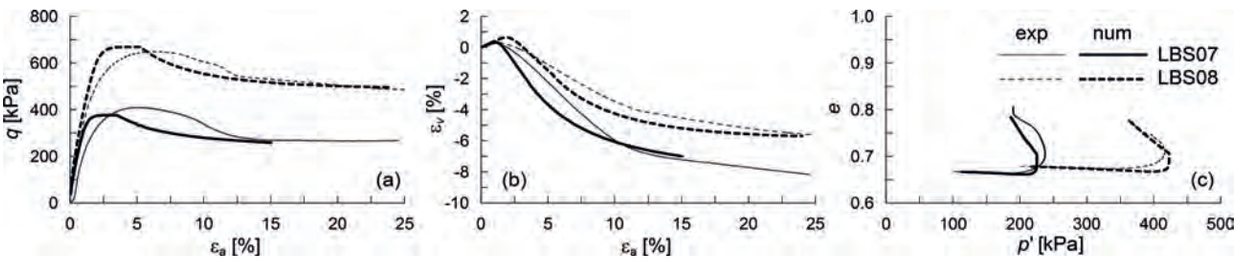

Fig. 5 – Comparison between numerical simulations and experimental data from monotonic drained triaxial tests on LB Sand.

Fig. 5 – Confronto tra le simulazioni numeriche e i dati sperimentali relativi a prove triassiali drenate su sabbia LB.

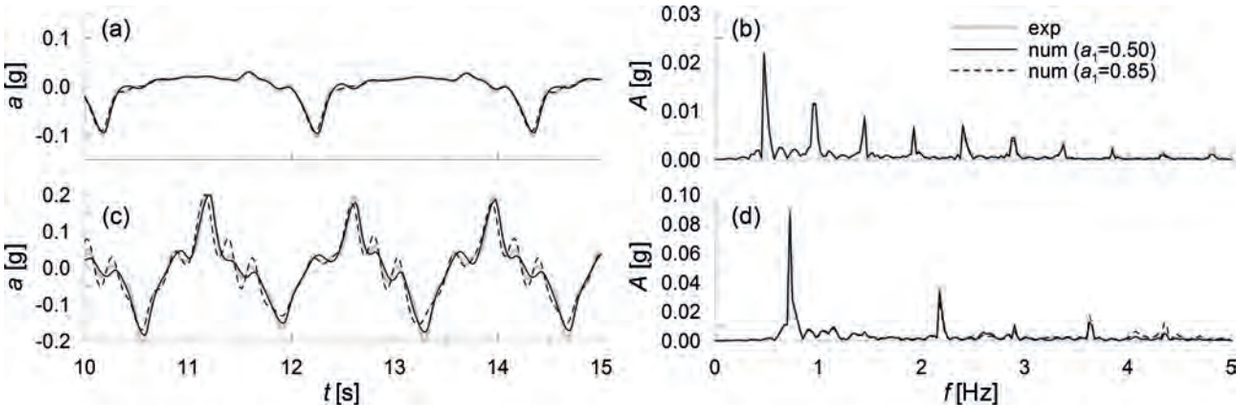

Fig. 6 – Test CW1: 1D wave propagation analyses for EQ1 a, b) and EQ4 c, d). Comparison between computed and recorded soil accelerations (accelerometer A6).

Fig. 6 – Test CW1: analisi di propagazione 1D relative ai terremoti EQ1 a, b) e EQ4 c, d). Confronto tra accelerazioni calcolate e misurate nel terreno (accelerometro A6).

During the swing-up stage, standard boundary conditions were applied to the model, *i.e.* zero horizontal displacements along the lateral boundaries and fixed nodes at the base of the grid. Following the same procedure adopted in the experiments, soil elements corresponding to the excavated volume were removed at 1 *g* and then the gravitational acceleration into the model was increased gradually from 1 *g* to 80 *g* in successive steps.

After the swing-up stage, static constraints were removed from the boundaries. The input acceleration time histories (A1) were applied to the bottom nodes of the grid, together with a zero velocity condition in the vertical direction. As in MADABHUSHI and ZENG [2007] and ATIK and SITAR [2010], periodic constraints were applied to the nodes on the lateral boundaries of the grid, *i.e.* they were tied to one-another in order to enforce the same displacements in both vertical and horizontal direction.

A time increment of $\Delta t = 1.0\times10^{-7}$ s (at model scale) was adopted in the analyses, in order to guarantee the stability of the explicit time integration scheme. Moreover, an additional viscous Rayleigh damping ($D = 5\%$ at $f = f_{inp}$) was used to overcome the high-frequency noise mainly due to the low value of hysteretic damping at small strains (see *e.g.* GHOSH and MADABHUSHI, 2003], but not otherwise affecting the results of the analyses.

Numerical results

Test CW1

With reference to earthquakes EQ2 and EQ5, figure 8 compares the computed and recorded time histories of the accelerations close to the free-field soil surface (A6), below dredge level (A15) and behind the left wall (A12), and of the dynamic increments of bending moment on the right wall ($z = 5.44$ m). Predicted and measured accelerations match almost perfectly, independently on the nominal fre-

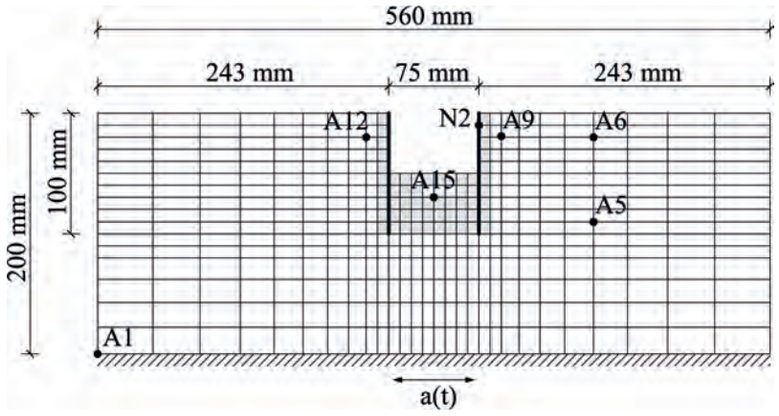

Fig. 7 – Mesh used in the 2D numerical analyses (model scale).

Fig. 7 – Griglia computazionale utilizzata nelle analisi 2D (scala del modello).

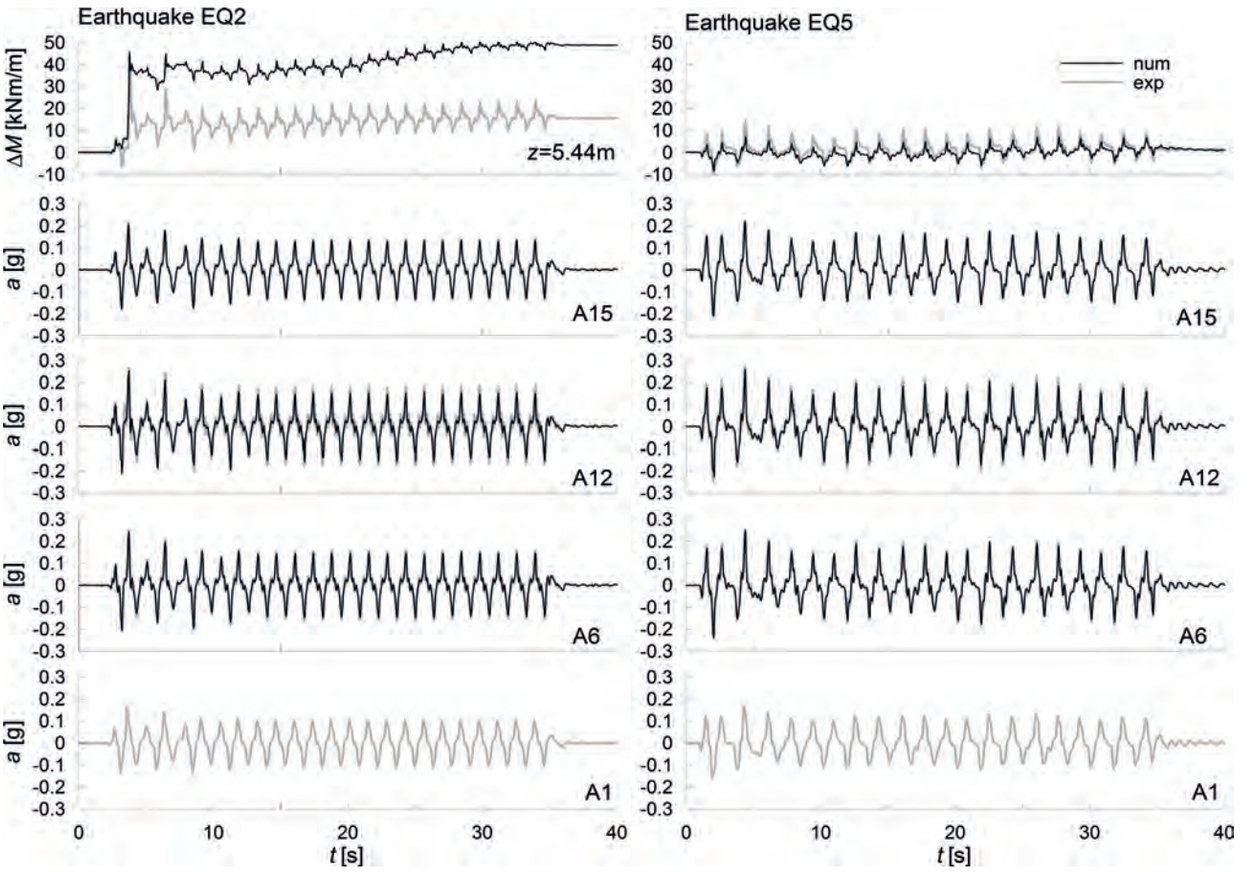

Fig. 8 – Test CW1, earthquakes EQ2 and EQ5. Dynamic bending moment on the right wall at z = 5.44m, accelerations at the base of the mesh (A1), at the top of the soil layer (A6), behind the left wall (A12) and below dredge level (A15). Comparison between experimental data and numerical results.

Fig. 8 – Test CW1, terremoti EQ2 e EQ5. Incremento dinamico di momento flettente nella paratia destra alla quota z = 5.44m, accelerazioni alla base del modello (A1), in prossimità della superficie dello strato di sabbia (A6), dietro il muro sinistro (A12) e a fondo scavo (A15). Confronto tra dati sperimentali e risultati numerici.

quency or amplitude of the applied signal. In both the numerical and the physical model, small amplifications between the bottom and the top of the soil layer are detected ($a_{max,A6}/\ a_{max,A1} \leq 1.6$) and no significant 2-D effects due to the presence of the walls ($a_{max,A12}/\ a_{max,A6} \leq 1.2$) or phase shift of accelerations into the model (see Tab. VI). Some discrepancies can be observed in terms of dynamic bending moments during earthquake EQ2, where the computed and measured residual values are 48 kNm/m and 15 kNm/m respectively, while a good agreement is recovered during EQ5, where no substantial increments are detected in both cases.

The difference between computed and measured internal forces is even more evident in figure 9, which shows the bending moment distribution on the left wall at the end of the swing-up stage (static) and of each earthquake (residual). Numerical predictions are significantly larger than experimental measurements. The maximum computed bending moment is 42 kNm/m in static conditions and increases up to 75 kNm/m and 130 kNm/m at the end of earthquakes EQ1 and EQ2 respectively. On the contrary, the corresponding experimental values are 37 kNm/m, 51 kNm/m and 62 kNm/m respectively. As discussed in CONTI *et al.* [2012], most of these discrepancies may be due to the presence of the electrical connections from the strain gauges in the physical model, which act as rotational and translational springs distributed along the mid section of the aluminium plates, and are not reproduced in the numerical simulations. Nonetheless, the behaviour exhibited by the wall is the same, that is it accumulates significant permanent bending moments only during the first two earthquakes.

Figure 10 shows the horizontal displacement time histories of the left wall, recorded by LV1 (z = 9 mm at model scale) and computed at node N2 (z = 10 mm) during the five earthquakes, that is neglecting the static component associated to the swing-up stage. The displacements computed at the end of EQ1, EQ2 and EQ4 are 9 mm, 17 mm and 16

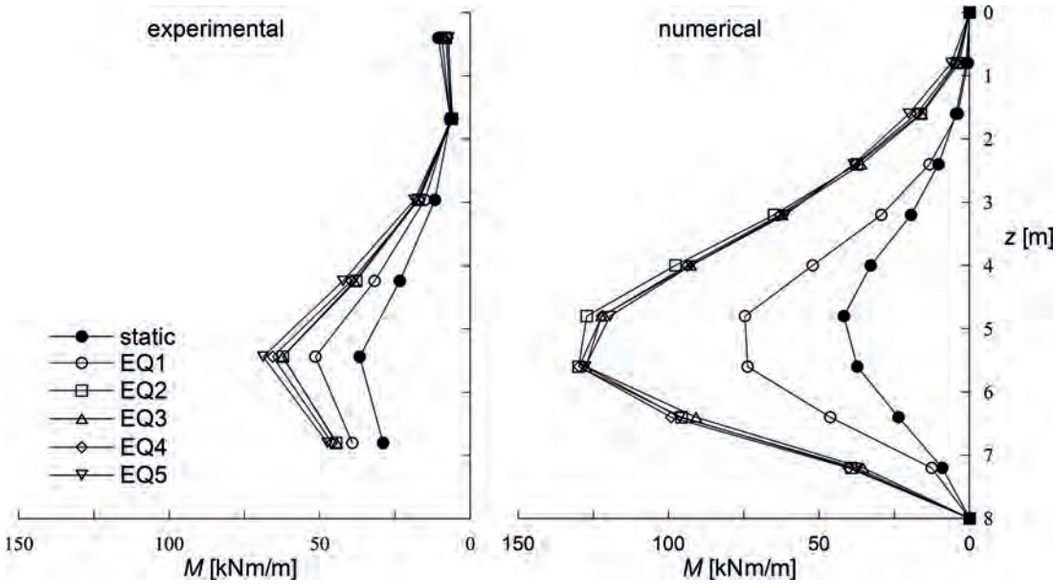

Fig. 9 – Test CW1: residual bending moments on the left wall at the end of each earthquake. Comparison between experimental data and numerical results.

Fig. 9 – Test CW1: momenti flettenti residui nella paratia sinistra al termine di ciascun terremoto. Confronto tra dati sperimentali e risultati numerici.

mm respectively, in quite good agreement with those measured in the centrifuge, that are equal to 13 mm, 21 mm and 14 mm respectively. No significant residual displacements are measured during earthquakes EQ3 and EQ5, while the corresponding values predicted by the numerical simulation are 3 mm and 10 mm respectively.

As shown in figure 11, which represents the deflection of the left wall at the end of the swing up and of the five earthquakes, the horizontal displacements measured in the centrifuge correspond mainly to rigid rotations, while they are affected significantly by the flexural bending of the wall in the numerical analyses, at least for the static stage and the

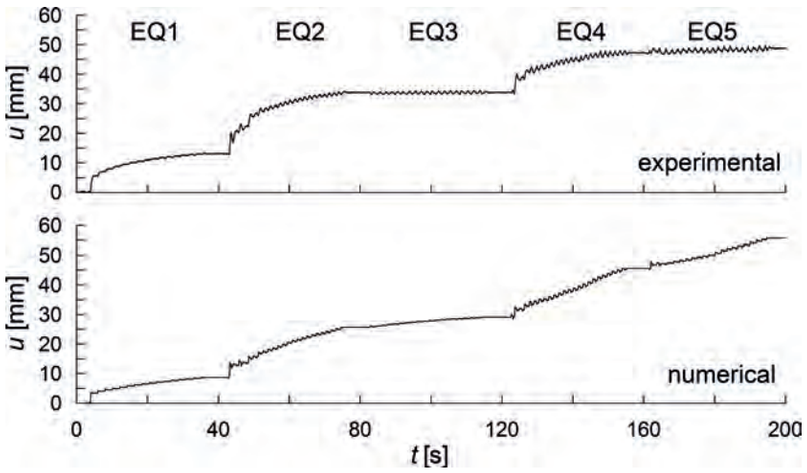

Fig. 10 – Test CW1: time history of the horizontal displacement near the top of the left wall. Comparison between experimental data and numerical results.

Fig. 10 – Test CW1: storia temporale degli spostamenti orizzontali in prossimità della sommità della paratia sinistra. Confronto tra dati sperimentali e risultati numerici.

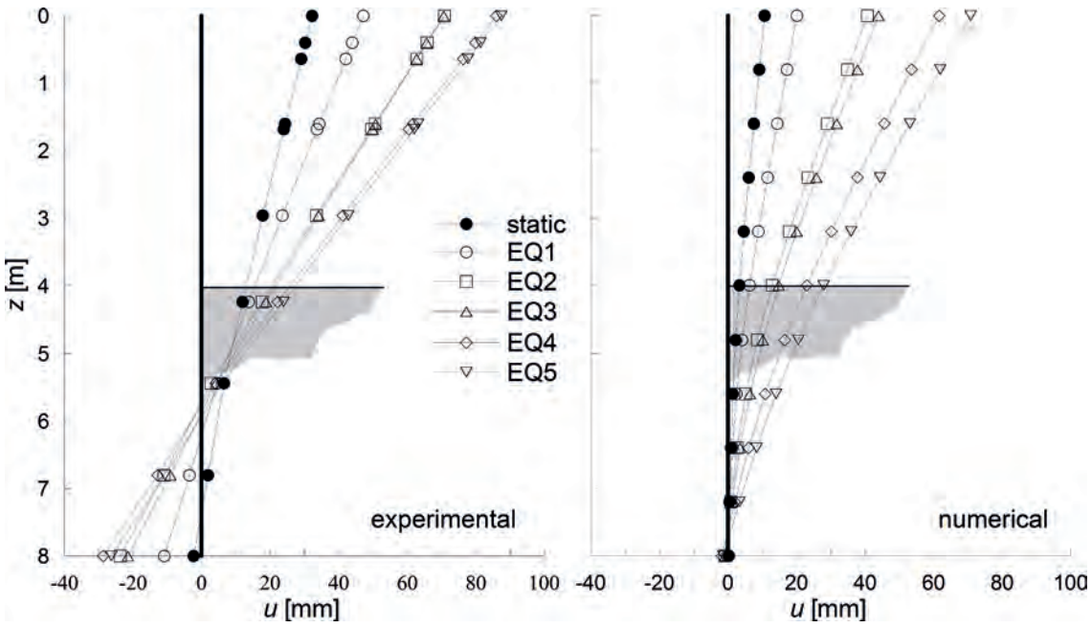

Fig. 11 – Test CW1: horizontal deflection of the left wall at the end of each earthquake. Comparison between experimental data and numerical results.
Fig. 11 – Test CW1: deformata della paratia sinistra al termine di ciascun terremoto. Confronto tra dati sperimentali e risultati numerici.

first two dynamic events. This evidence, already observed by MADABHUSHI and ZENG [2007], may be related partly to the difference between measured and computed bending moments or to local disuniformities of the sand in the physical model close to the toe of the walls. Again, the observed phenomenon is the same in both the physical and the numerical model, *i.e.* permanent displacements experienced by the wall during earthquakes EQ3 and EQ5 are much smaller than those accumulated during EQ1 and EQ2 respectively, even if they are characterised by larger peak accelerations (see Tab. VI).

As discussed in CONTI *et al.* [2012], both permanent displacements and residual bending moments in the walls depend on the entire acceleration time history the system has ever experienced, and not only on the current earthquake intensity. Two aspects are of major concern: (i) even small earthquakes, such as EQ1, can induce permanent deformations in the system; (ii) a dynamic event, such as EQ3 and EQ5, produces neither permanent increments of the internal forces nor significant displacements if a stronger earthquake has occurred before. According to CONTI *et al.* [2012], this behaviour does not depend on the tendency of the sand to densify when vibrated, rather on a redistribution of the stress state around the excavation during shaking.

Figure 12 shows the soil contact stresses at the end of the swing up stage and of each earthquake, together with the static active and passive limit values ($\phi = \phi_{cv}$) computed according to LANCELLOTTA [2002]. Although the excavation stage was not simulated in the model, the static stress distribution is quite similar to that observed in the numerical simulation of ideal excavations in homogeneous sand layers [CALLISTO, 2014; CONTI *et al.*, 2014]: the soil behind the walls is in active limit state down to about 5 m from the surface, while in front of the walls the passive resistance is fully mobilised only immediately below dredge level, the horizontal stresses being approximately constant at higher depths. During earthquakes EQ1 and EQ2, the inertia forces into the soil induce an increment of contact stresses behind the walls and, as a consequence, a progressive rotation of the walls concurrently with a mobilization of the passive resistance of the soil below dredge level. The stronger the accelerations applied, the larger the rotation of the walls and the greater the depth down to which the passive resistance of the soil is fully mobilised. This process clearly results in a substantial increment of residual bending moments in the walls. At the end of EQ2 the stress state in front of the wall is such that, during the subsequent (lower) earthquake EQ3, neither redistribution of contact stresses nor significant rotation of the walls take place. On the contrary, during the subsequent stronger earthquake EQ4, the progressive rotation of the walls seems to be due mainly to a reduction of the soil friction angle with increasing cyclic deformation, rather than to a deeper mobilization of passive resistance below dredge level, resulting in a negligible increment of residual bending moments. Finally, the behaviour observed during EQ5 is substantially the same of earthquake EQ3.

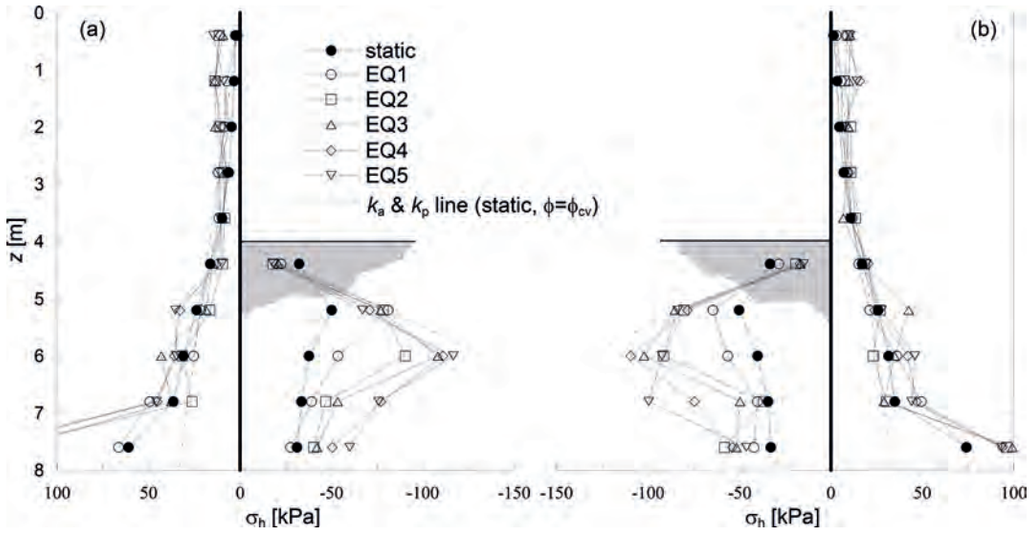

Fig. 12 – Test CW1, numerical results: earth pressure distribution at the end of each earthquake behind a) left and b) right wall.
Fig. 12 – Test CW1, risultati numerici: distribuzione delle tensioni di contatto al termine di ciascun terremoto dietro la paratia a) sinistra e b) destra.

Test CW2

Figure 13 shows, for earthquakes EQ1 and EQ3, a comparison between computed and recorded time histories of the accelerations below dredge level (A15) and behind the left wall (A12), and of the dynamic increments of bending moment on the right wall (z = 5.44 m). As for test CW1, there is an almost perfect agreement between predicted and measured accelerations, while some differences can be observed in terms of dynamic bending moments, especially during earthquake EQ2, where the computed and measured residual values are 18 kNm/m and 8 kNm/m respectively.

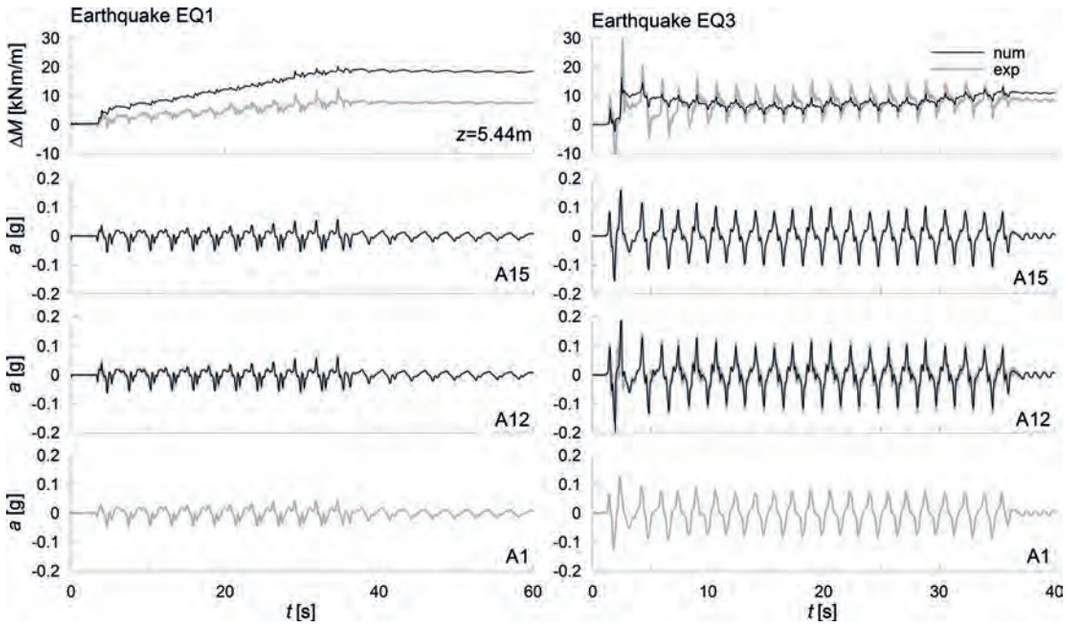

Fig. 13 – Test CW2, earthquakes EQ1 and EQ3. Dynamic bending moment on the right wall at z = 5.44m, accelerations at the base of the mesh (A1), behind the left wall (A12) and below dredge level (A15). Comparison between experimental data and numerical results.
Fig. 13 – Test CW2, terremoti EQ1 e EQ3. Incremento dinamico di momento flettente nella paratia destra alla quota z = 5.44m, accelerazioni alla base del modello (A1), dietro il muro sinistro (A12) e a fondo scavo (A15). Confronto tra dati sperimentali e risultati numerici.

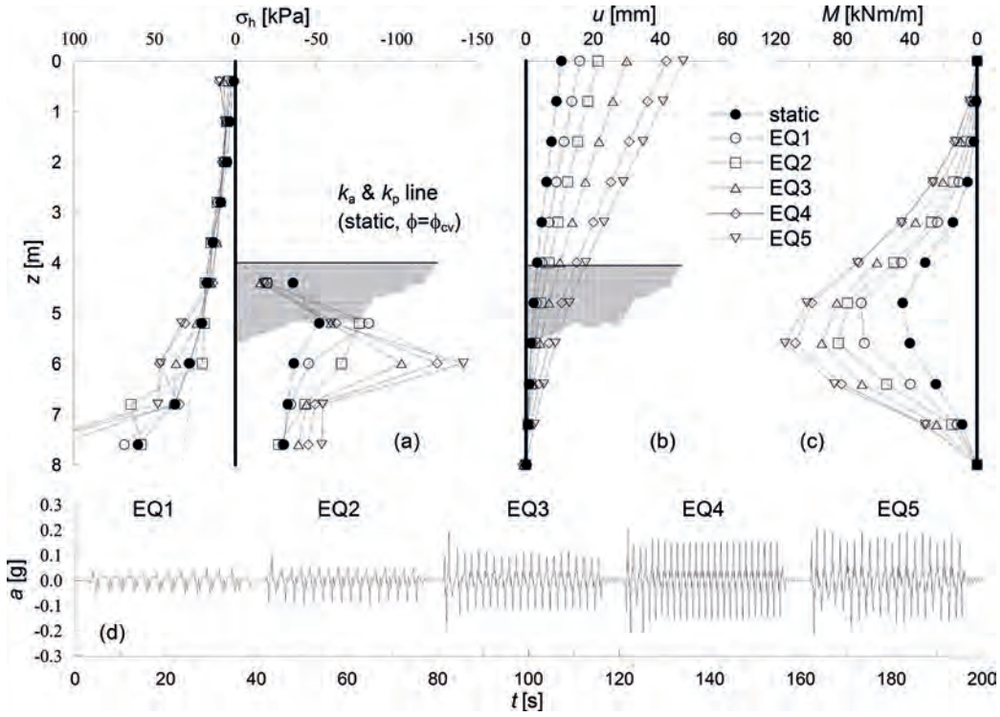

Fig. 14 – Test CW2, numerical results: a) earth pressure distribution, b) horizontal displacements, c) bending moments on the left wall at the end of each earthquake and d) acceleration time histories behind the left wall (A12).
Fig. 14 – Test CW2, risultati numerici: a) distribuzione delle tensioni di contatto, b) spostamenti orizzontali, c) momenti flettenti nella paratia sinistra al termine di ciascun terremoto e d) storia temporale dell'accelerazione a tergo della paratia sinistra (A12).

Figure 14 shows a comprehensive view of the main numerical results concerning the dynamic behaviour of the left wall, that is: (a) the horizontal contact stress distribution, (b) the horizontal deflection and (c) the bending moment distribution at the end of each stage and (d) the acceleration time history computed behind the left wall (A12). Unlike test CW1, the applied earthquakes are characterised by increasing maximum accelerations (see also Tab. VI). As a result, during each stage inertia forces into the soil produce a progressive rotation of the wall, concurrently with a progressive mobilization of the soil passive resistance below dredge level and a permanent increase of the internal forces in the structure.

Figure 15 shows (a) the bending moment distribution and (b) the permanent rotation of the left wall measured at the end of each earthquake. No LVDT measurements were available for test CW2, therefore rotations were obtained from the recordings of the horizontal MEMS accelerometers located on the top of the walls (M3, M4). By comparing figure 14c and figure 15a it is apparent, again, that the internal forces predicted by the numerical analysis are significantly larger than the experimental measurements, the maximum bending moment computed at the end of the test (EQ5) being about 1.5 times the recorded one. Nonetheless, it is noteworthy that the behaviour observed in both the physical and the numerical model is the same, in terms both progressive rotation and accumulation of permanent bending moment in the wall.

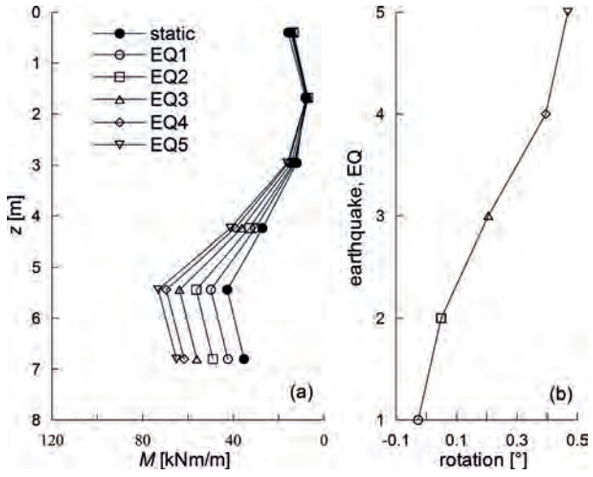

Fig. 15 – Test CW2, experimental data: a) residual bending moments and b) rotation of the left wall at the end of each earthquake.
Fig. 15 – Test CW2, dati sperimentali a) momenti flettenti residui e b) rotazione della paratia sinistra al termine di ciascun terremoto.

Conclusions

This work dealt with the numerical simulation of two dynamic centrifuge tests on cantilevered retaining walls in dry sand. The results demonstrate that numerical modelling can provide a good description of the seismic response of retaining walls, where soil-structure interaction phenomena play a major role. Moreover, the advanced constitutive model succeeded in capturing the mechanical response of the sand under cyclic loading, for different values of the initial relative density. While very good agreement has been obtained between computed and measured accelerations into the soil, some discrepancies have been observed in terms of displacements and bending moments into the walls, the latter being due mainly to secondary experimental factors not taken into account in the numerical analyses.

Numerical results have shown that the dynamic behaviour of embedded cantilevered retaining walls is strongly related to the redistribution of the stress state around the excavation induced by the inertia forces into the soil. More specifically, permanent rotations of the wall induce a progressive mobilization of the soil passive resistance, starting from the dredge level, and a consistent increase of the internal forces into the wall. Furthermore, the analyses have confirmed that significant displacements can be attained during an earthquake even for maximum accelerations lower than the limit equilibrium critical value.

The initial stress distribution at the contact between the soil and the wall is, therefore, one of the key factors governing the seismic behaviour of embedded cantilever walls. Remarkably, as the numerical static distribution was not affected by the particular procedure followed to simulate the swing-up stage, the main conclusions of the paper would apply also to real problems. As a matter of fact, the same phenomena described in this paper have been observed in a number of parametric numerical studies on the behaviour of cantilevered walls during real earthquakes [Conti and Viggiani, 2013; Conti *et al.*, 2014], thus confirming the general validity of the conclusions just outlined. However, the results are limited to the dynamic behaviour of retaining walls in dry sand, so further research is needed to investigate the influence of pore water pressure on the seismic response of such structures.

Acknowledgements

The research presented in this paper was developed with the financial support of the Italian Department of Civil Protection within the ReLUIS research project. The Author wishes to express his gratitude to Giulia Viggiani for her precious advise. The routine for the constitutive soil model was kindly provided by Professor George Bouckovalas and Professor Achilleas Papadimitriou, who are also gratefully acknowledged.

References

Andrianopoulos, K.I., Papadimitriou A.G., Bouckovalas G.D. (2010a) – *Bounding surface plasticity model for the seismic liquefaction analysis of geostructures.* Soil Dyn. Earthquake Eng., 30, n. 10, pp. 895-911.

Andrianopoulos, K.I., Papadimitriou A.G., Bouckovalas G.D. (2010b) – *Explicit integration of bounding surface model for analysis of earthquake soil liquefaction.* Int. J. Num. Anal. Meth. Geomech., 34, n. 15, pp. 1586-1614.

Atik L.A., Sitar N. (2010) – *Seismic earth pressures on cantilever retaining structures.* J. Geotech. Geoenv. Eng., 136, n. 10, pp. 1324-1333.

Aversa S., de Sanctis L., Maiorano R.M.S., Tricarico M., Viggiani G.M.B., Conti R., Madabhushi G.S.P. (2015) – *Centrifuge modelling of retaining walls embedded in saturated sand under seismic actions.* Geotechnical, Geological and Earthquake Engineering, 35, pp. 543-562.

Been K., Jefferies M.G. (1985) – *A state parameter for sands.* Géotechnique, 35, n. 2, pp. 99-112.

Callisto L., Soccodato F.M., Conti R. (2008) – *Analysis of the Seismic Behaviour of Propped Retaining Structures.* Proc. Earthquake Engineering and soil Dynamics, IV Conf., Sacramento.

Callisto L. (2014) – *Capacity design of embedded retaining structures.* Géotechnique, 64. n. 3, pp. 204-214.

Cilingir U., Haigh S.K., Madabhushi S.P.G., Zeng X. (2011) – *Seismic behaviour of anchored quay walls with dry backfill.* Geomechanics and Geoengineering, 6, n. 3, pp. 227-235.

Conti R. (2010) – *Modellazione fisica e numerica del comportamento di opere di sostegno flessibili in condizioni sismiche.* PhD thesis, Università degli Studi di Roma Tor Vergata, Roma, Italy (in italian).

Conti R., Viggiani G.M.B. (2012) – *Evaluation of soil dynamic properties in centrifuge tests.* J. Geotech. Geoenv. Eng., 138, n. 7, pp. 850-859.

Conti R., Madabhushi S.P.G., Viggiani G.M.B. (2012) – *On the behaviour of flexible retaining walls under seismic actions.* Géotechnique, 62, n. 12, pp. 1081-1094.

Conti R., Viggiani G.M.B. (2013) – *A new limit equilibrium method for the pseudostatic design of embedded cantilevered retaining walls.* Soil Dyn. Earth. Eng., 50, pp. 143-150.

Conti R., Viggiani G.M.B., Cavallo S. (2013) – *A two-rigid block model for sliding gravity retaining walls.* Soil Dyn. Earth. Eng., 55, pp. 33-43.

Conti R., Viggiani G.M.B, Burali d'Arezzo F. (2014) – *Some remarks on the seismic behaviour of embedded cantilevered retaining walls.* Géotechnique, 64, n. 1, pp. 40-50.

DAY R.W. (2002) – *Geotechnical earthquake engineering handbook*. McGraw-Hill.

DEWOOLKAR M.M., KO H.Y., PAK R.Y.S. (2001) – *Seismic behavior of cantilever retaining walls with liquefiable backfills*. J. Geotech. Geoenviron. Eng., 127, n. 4, pp. 424-435.

DEWOOLKAR M.M., CHAN A.H.C., KO H.Y., PAK R.Y.S. (2009) – *Finite element simulations of seismic effects on retaining walls with liquefiable backfills*. Int. J. Num. Anal. Meth. Geomech., 33, pp. 791-816.

FANG Y.S., YANG Y.C., CHEN T.J. (2003) – *Retaining walls damaged in the Chi-Chi earthquake*. Can. Geotech. J., 40, pp. 1142-1153.

GHOSH B., MADABHUSHI S.P.G. (2003) – *A numerical investigation into effects of single and multiple frequency earthquake input motion*. Soil Dyn. Earthquake Eng., 23, n. 8, pp. 691-704.

ILANKATHARAN M., KUTTER B.L. (2008) – *Numerical simulation of soil model-model container-centrifuge shaking Table system*. Proc. Earthquake Engineering and soil Dynamics, IV Conf., Sacramento.

ITASCA (2005) – *FLAC Fast Lagrangian Analysis of Continua* v. 5.0. User's Manual.

KONTOE S., ZDRAVKOVIC L., POTTS D.M. (2009) – *An assessment of the domain reduction method as an advanced boundary condition and some pitfalls in the use of conventional absorbing boundaries*. Int. J. Numer. Anal. Meth. Geomech., 33, pp. 309-30.

KONTOE S., ZDRAVKOVIC L., POTTS D.M. (2008) – *An assessment of time integration schemes for dynamic geotechnical problems*. Comput. Geotech., 35, n. 2, pp. 253-64.

KUHLEMEYER R.L., LYSMER J. (1973) – *Finite element method accuracy for wave propagation problems*. J. Soil Mech. & Foundations, ASCE, 99, SM5, pp. 421-427.

KWOK A.O.L., STEWART J.P., HASHASH Y.M.A., MATASOVIC N., PYKE R., WANG Z., YANG Z. (2007) – *Use of exact solutions of wave propagation problems to guide implementation of nonlinear seismic ground response analysis pro*cedures. J. Geotech. Geoenv. Eng., 133, n. 11, pp. 1385-1398.

LANCELLOTTA R. (2002) – *Analytical solution of passive earth pressure*. Géotechnique, 52, n. 8, pp. 617-619.

LING H.I., LIU H., KALIAKIN V., LESHCHINSKY D. (2004) – *Analysing dynamic behavior of geosynthetic-reinforced soil retaining walls*. J. Eng. Mech., 130, n. 8, pp. 911-920.

MADABHUSHI S.P.G., ZENG X. (2007) – *Simulating Seismic Response of Cantilever Retaining Walls*. J. Geotech. Geoenv. Eng., 133, n. 5, pp. 539-549.

MANZARI M.T., DAFALIAS Y.F. (1997) – *The strength and dilatancy of sands*. Géotechnique, 47, n. 2, pp. 255-272.

MARKETOS G., MADABHUSHI S.P.G. (2004) – *An investigation of the failure mechanism of a cantilever retaining wall under earthquake loading*. Int. J. Phys. Model. Geotech., 4, n. 4, pp. 33-44.

MUIR WOOD D. (2004) – *Geotechnical modelling*. Spon Press (Taylor and Francis Group).

NEWMARK N.M. (1965) – *Effects of earthquakes on dams and embankments*. Géotechnique, 15, n. 2, pp. 139-160.

PAPADIMITRIOU A.G., BOUCKOVALAS G.D. (2002) – *Plasticity model for sand under small and large cyclic strains: a multiaxial formulation*. Soil Dyn. Earthquake Eng., 22, n. 3, pp. 191-204.

PAPADIMITRIOU A.G., BOUCKOVALAS G.D., DAFALIAS Y.F. (2001) – *Plasticity model for sand under small and large cyclic strains*. J. Geotech. Geoenv. Eng., 127, n. 11, pp. 973-983.

PIANC (2001) – *Seismic Design Guidelines for Port Structures*. Working Group n. 34 of the Maritime Navigation Commission, International Navigation Association, Balkema, Rotterdam.

RICHARDS R., ELMS D.G. (1979) – *Seismic behaviour of gravity retaining walls*. J. Geotech. Eng. Div., ASCE, 105, n. 4, pp. 449-464.

TAN F.S. (1990) – *Centrifuge and Theoretical Modelling of Conical Footings on Sand*. PhD Thesis, University of Cambridge, Cambridge, UK.

VELACS – *Verification of numerical procedures for the analysis of soil liquefaction problems*. (1993) – Proc. Int. Conf. "Verification of Numerical Procedures for the Analysis of Soil Liquefaction Problems", K. Arulanandan and F. Scott, (Eds.), Davis, Cali.

VISONE C. (2008) – *Performance-based design approach in seismic design of embedded retaining walls*. PhD Thesis, Università degli Studi di Napoli Federico II, Naples, Italy.

VUCETIC M., DOBRY R. (1991) – *Effect of soil plasticity on cyclic response*. J. Geotech. Geoenv. Eng., 117, n. 1, pp. 89-107.

VUCETIC M. (1994) – *Cyclic threshold shear strains in soils*. J. Geotech. Geoenv. Eng., 120, n. 12, pp. 2208-2228.

WHITMAN R.V. (1990) – *Seismic design and behaviour of gravity retaining walls*. Design and Performance of Earth Retaining Structures, ASCE, Geotech. Special Publication, 25, pp.817-842.

ZENG X., SCHOFIELD A.N. (1996) – *Design and performance of an equivalent-shear-beam container for earthquake centrifuge modelling*. Géotechnique, 46, n. 1, pp. 83-102.

ZENG X., STEEDMAN R.S. (2000) – *Rotating block method for seismic displacement of gravity walls*. J. Geotech. Geoenv. Eng., 126, n. 8, pp. 709-717.

ZHANG J.M., WANG G. (2012) – *Large post-liquefaction deformation of sand, part I: physical mechanism, constitutive description and numerical algorithm*. Acta Geotechnica, 7, n. 2, pp.69-113.

ZIENKIEWICZ O.C., BIANIC N., SHEN F.Q. (1988) – *Earthquake input definition and the transmitting boundary condition*. Conf: "Advances in computational non-linear mechanics", St. Doltnis (Ed.) I, pp. 109-138.

Modellazione numerica di prove dinamiche in centrifuga su modelli in scala ridotta di paratie a sbalzo

Sommario

Questo articolo presenta i risultati della modellazione numerica di due prove dinamiche in centrifuga eseguite su coppie di paratie a sbalzo a sostegno di uno scavo in sabbia asciutta, ricostituita a due valori differenti di densità relativa. Sono state eseguite analisi numeriche in stato piano di deformazione, utilizzando un modello costitutivo avanzato per il terreno, i cui parametri sono stati tarati sulla base dei risultati di prove di laboratorio convenzionali. I risultati ottenuti mostrano che la modellazione numerica fornisce una descrizione accurata del comportamento sismico di paratie a sbalzo: si è ottenuto un accordo molto buono tra previsioni numeriche e dati sperimentali in termini di accelerazioni, mentre sono state osservate discrepanze in termini di spostamenti e momenti flettenti nelle paratie, principalmente da ascriversi a fattori sperimentali che non sono stati modellati nelle analisi numeriche. Il comportamento dinamico delle paratie a sbalzo è strettamente legato alla ridistribuzione di stato tensionale indotta nell'intorno dello scavo per effetto delle azioni inerziali agenti nel terreno. Più in particolare, le rotazioni permanenti della paratia inducono una progressiva mobilitazione della resistenza passiva nel terreno situato a valle e, conseguentemente, un incremento di momento flettente. Inoltre, un terremoto può indurre spostamenti significativi anche se caratterizzato da un'accelerazione massima più piccola rispetto all'accelerazione critica del sistema.